Chemosphere 208 (2018) 740–748

Contents lists available at ScienceDirect

Chemosphere

journal homepage: www.elsevier.com/locate/chemosphere

Characterization of phosphorus availability in response to radial oxygen losses in the rhizosphere of *Vallisneria spiralis*

Chao Han [a], Jinghua Ren [b], Zhaode Wang [a, *], Shika Yang [a], Fan Ke [a], Di Xu [a], Xianchuan Xie [c, **]

[a] State Key Laboratory of Lake Science and Environment, Nanjing Institute of Geography and Limnology, Chinese Academy of Sciences, Nanjing, 210008, China
[b] Geological Survey of Jiangsu Province, Nanjing, 210018, China
[c] State Key Laboratory of Pollution Control and Resource Reuse, School of the Environment, Nanjing University, Nanjing, 210093, China

HIGHLIGHTS

- DO concentration and P flux in *V. spiralis* rhizosphere were imaged simultaneously.
- Observed heterogeneous co-distribution of O_2 and P availability, mediated by roots.
- Diurnal rhythms of O_2 and P availability around *V. spiralis* roots were documented.
- Direct evidence showed unequivocal P immobilization affected by radial oxygen loss.

GRAPHICAL ABSTRACT

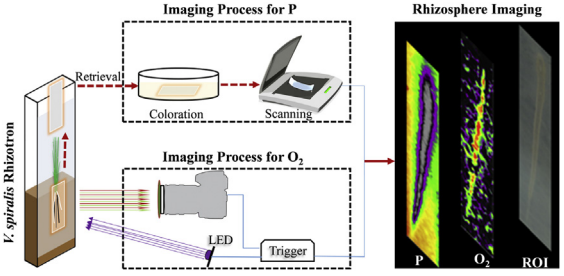

ARTICLE INFO

Article history:
Received 10 February 2018
Received in revised form
23 May 2018
Accepted 29 May 2018
Available online 1 June 2018

Handling Editor: X. Cao

Keywords:
Microscale imaging
O_2 availability
Labile P flux
Diurnal rhythm
Rhizosphere

ABSTRACT

The viewpoint that radial oxygen loss (ROL) of submerged macrophytes induces changes in redox conditions and the associated phosphorus (P) availability has been indirectly confirmed at larger spatial scales using conventional, destructive techniques. However, critical information about microniches has largely been overlooked due to the lack of satisfactory *in situ* mapping technologies. In this study, we deployed a recently developed hybrid sensor in the rhizosphere of *Vallisneria spiralis* (*V. spiralis*) during two vegetation periods to provide 2-D imaging of the spatiotemporal co-distribution of oxygen (O_2) and P from a fixed observation point. Overall, the images of O_2 and P showed a high degree of spatiotemporal heterogeneity throughout the rhizosphere at the sub-mm scale. A clear decrease in the P mobilization corresponded well to the steep O_2 enhancement within a 2-mm-thick zone around younger *V. spiralis* root, indicating a significant coupling relationship between ROL and P availability. Surprisingly, despite significant diurnal shifts in ROL along the older *V. spiralis* roots, P availability did not fluctuate in a substantial part of the rhizosphere throughout the day; however, ROL increased the P immobilization significantly by changing the redox gradients at the outer rhizosphere. This study clearly demonstrates how continuous ROL of *V. spiralis* can play a major role in regulating P availability within the rhizosphere. The premise behind this statement is the discovery of how this continuous ROL can lead to the formation of three distinctive redox landscapes in the rooting sediment (oxic, suboxic, or anaerobic layers).

* Corresponding author.
** Corresponding author.
E-mail addresses: zdwang@niglas.ac.cn (Z. Wang), xchxie@nju.edu.cn (X. Xie).

https://doi.org/10.1016/j.chemosphere.2018.05.180
0045-6535/

1. Introduction

Rhizosphere environments are the most active portions of aquatic/terrestrial ecosystems, in which intense biogeochemical processes within microniches may strongly impact biogeochemical cycles even up to the global scale (Hoefer et al., 2017; Kuzyakov and Blagodatskaya, 2015; Razavi et al., 2016). Accordingly, rhizosphere micro-interfacial processes and interactions have attracted the attention of researchers for decades. However, rhizosphere environments, especially those of macrophytes, exhibit a high spatio-temporal heterogeneity, and most processes involve changes in two or more parameters (Luo et al., 2010; Williams et al., 2014). To learn more, it is desirable to measure the relevant biogeochemical parameters simultaneously at the microscale level and at exactly the same position.

Phosphorus (P) has always been considered indispensable to algae, bacteria, and macrophyte growth, and its availability is generally believed to determine productivity in most freshwater systems (Schelske, 2009). However, too much P in water bodies can cause serious eutrophication and eventually promote prolonged hypoxia, destroying the ecological balance (Han et al., 2015). Because P contamination can migrate from the sediment into the water, controlling internal P loads has been a major goal in maintaining the trophic status of water bodies (Sondergaard et al., 2003). Previous studies of European and North American lakes have shown that internal P migration is intense and persistent (typically 10–15 years) (Sondergaard et al., 2013). Accordingly, understanding the status of P within sediments is crucial for managing or recovering a eutrophic lake. Although many factors are involved in this process, the redox-controlled mobilization and retention of P and microbial processes within the sediments are considered particularly important.

Many macrophytes, such as *V. spiralis*, have been used in constructed wetlands to control P release from hypereutrophic waters (Ke and Li, 2006; Soana and Bartoli, 2013). Among the several P-control mechanisms, radial oxygen loss (ROL), plays an important role in regulating the P cycle within the macrophyte rhizosphere. As a key biological function of macrophytes, the ROL-derived O_2 leakage from roots can diffuse several millimeters out into the surrounding sediment, creating a mosaic of oxidized zones deep in the rhizosphere (Armstrong et al., 2000; Koop-Jakobsen et al., 2017), which is essential to the long-term survival of macrophytes rooted in highly anoxic, toxic waterlogged sediments (Han et al., 2016; Jensen et al., 2005). Numerous studies have shown that macrophyte-derived ROL can actively reshape heterogeneous oxidation-reduction micro-environments, thereby contributing to P retention and mobilization in the adjacent sediment via geochemical speciation shifts (Cheng et al., 2014; Han et al., 2017). Nevertheless, most researches to date have primarily focused on establishing the relationship of various P fractions in the root-adjacent sediment and the total ROL sequestered using traditional methods based on the entire plant biomass (Lai et al., 2012; Cheng et al., 2014; Mei et al., 2014). Clear and direct evidence of the ROL role in driving the P mobilization and immobilization within the rhizosphere is scarce. This is because such evidence requires investigation into the rhizospheric micro-environment and its chemical activity on a fine, submillimeter (sub-mm) scale. Until now, the *in situ* technologies needed for such an investigation have not been fully accessible or utilized.

The unique conditions around the roots are highly heterogeneous in both space and time; thus, small-scale studies on dynamic processes occurring around the roots have always been technically challenging (Luo et al., 2014; Santner et al., 2015). Until recently, most available approaches for investigating chemical distributions involved *ex situ* plant/sediment sampling and handling, using porewater extraction and analysis by potentiometric or single-point titration (Huang et al., 2015; Cao et al., 2016). The disruptive procedures involved in these extractions and analyses naturally disturb the conditions of those biogeochemical gradients, which inhabit the narrow regions, preventing accurate determination of analyte distribution at relevant spatial scales in the rhizosphere (Guan et al., 2016; Zhou et al., 2016). Furthermore, the traditional protocols could only provide point measurements or one-dimensional (1-D) profiles, which can misrepresent the biogeochemical processes within the rhizosphere (Pages et al., 2011). More recently, two emerging *in situ* monitoring methods: the diffusive gradients in thin films (DGT) technique and planar optode (PO) technique have proven capable of capturing the spatiotemporal heterogeneity of the rhizosphere (Santner et al., 2012; Williams et al., 2014; Larsen et al., 2015). DGT is established based on Fick's First Law of Diffusion. Like a plant root, it removes chemical species (e.g. P) from pore water and induces resupply from the solid phase (Luo et al., 2018). While, the measuring principle of a planar O_2 optode, for example, is based on the dynamic quenching of the characteristic luminescence by O_2 upon light excitation with no O_2 consumption (Han et al., 2016). Both have considerable benefits over currently available methods such as being economically accessible, low-disturbance sampling, selectivity and sensitivity, high spatial measurement (Liang et al., 2014; Pan et al., 2015; Santner et al., 2015). A few researchers have successfully used PO and DGT methods in parallel to study the relevant biogeochemical processes associated with P/O_2 in heterogeneous rhizosphere (Williams et al., 2014; Brodersen et al., 2017). To our best knowledge, detailed information on the direct interaction between P and O_2 availability as well as the spatial and temporal co-distributions around the same individual roots from a microscale view is sparse.

V. spiralis is a perennial and common submersed macrophyte species, thrives in most shallow lakes in China, and thus, were selected as the living test organisms in this study. To explore the dynamics of O_2 and P availability and their interactions in the rhizosphere of *V. spiralis* in more detail, we quantitatively imaged the co-distributions of dissolved oxygen (DO) concentrations and labile P fluxes near the roots of *V. spiralis* over a daylong cycle and considered the potential effect of P mobilization in response to ROL. To achieve this, we used a recently-developed DGT-optode sensor (DOS)—a novel imaging system that combines an optical O_2 sensor and colorimetric DGT—to create noninvasive chemical images of labile P fluxes and DO concentrations near the *V. spiralis* roots at spatial resolutions down to sub-mm scales.

2. Materials and methods

2.1. Samples collection and preparation

On 12 June 2017, macrophyte specimens of *V. spiralis* and sediment for the pot experiment were collected from the mesotrophic zone in Gonghu Bay of Lake Taihu (31°23′22.3″N; 120°20′45.4″E), where a moderately dense but patchy macrophyte cover thrives. The *V. spiralis* were harvested by digging out intact sediment blocks that were gently washed to remove any sediment particles and benthic animals that adhered to them. They were subsequently taken to the greenhouse, where they were maintained in aerated water and provided a photoperiod with a daily cycle of 12-h light/12-h darkness by a tungsten halogen lamp and a constant ambient temperature of 25 °C. Tillers for the young *V. spiralis* were selected and were used in subsequent experiments. Sediment cores were collected with a 9.1 × 70 cm cylindrical sediment sampler, and only the upper 10 cm horizon was removed. Subsamples were then

transported to the laboratory, where they were sieved (using a mesh size of 2 mm) and homogenized thoroughly.

2.2. Preparation of rhizotron experiments

In this experiment, acrylic rhizotrons with detachable front plates were used to cultivate the experimental plants to enable a view of the rhizosphere processes (Koop-Jakobsen and Wenzhofer, 2015). The inner dimensions of the rhizotrons were 50 cm × 15 cm × 2 cm in height, width and depth, respectively. Before the sediments and plants were transported, the experimental front plates of the rhizotrons were carefully washed with ultra-pure nitric acid (5 percent v/v) and double-distilled water. The inside of the pre-cleaned plates were then smoothly overlaid by the 10 μm-thick hydrophilic polycarbonate membranes (0.4 μm pore size, areas of 40 cm × 15 cm) and attached firmly with waterproof tape at the U-shaped sides. The membrane not only was used to support the roots and sediments when DOS was deployed, but also served as a diffusive layer and prevented fouling by the sediment. The open side was then closed by mounting the front plates tightly onto the rhizotrons with 13 screws.

For the rhizosphere studies, the homogenized sediment was carefully poured into the rhizotrons and gently shaken, assuring a uniform distribution without gas bubbles from the sediment. Afterward, the collected lake water was gently added to the sediment surface using intravenous needles. Each rhizotron was filled with a layer of sediment 20 cm thick and overlying water 25 cm deep. The rhizotrons were left undisturbed in the greenhouse for seven days to allow the sediment to resettle and establish stable biogeochemical conditions within the sediment. Thereafter, the *V. spiralis* selected for study were gently transplanted to spots close to the front plates of the rhizotrons, and the whole system was moved on an oblique tray with an angle of incidence below 30° in the greenhouse to encourage root growth along the front plates due to gravitropism. Each rhizotron bottom was wrapped with aluminum foil to avoid potential interference from ambient light along the walls of the sediment cores or roots. Stirring and aeration of the water column was obtained via a submerged Pasteur pipet connected to an air pump or a gas mixer.

2.3. Noninvasive imaging of DO and labile P using DOS

DOS, a recently developed DGT-optode hybrid sensor, was deployed as an *in situ* technique for imaging the spatial co-distributions of DO and labile P around the roots during two vegetation periods (3 and 21 days). The preparation and measuring principle of the DOS are reported in Supporting Information Note 1. The schematic overview of the experimental design and imaging processes are presented in Fig. 1. Briefly, after appropriate root development, the region of interest (ROI) where several visually discernible roots were growing across the front plates, was identified and marked by sketching directly on the detachable plate. Afterward, the rhizotron was turned vertically, and the DOS sensing gel was then gently inserted through the gap between the front window and polycarbonate membrane to reach the ROI. Then the rhizotron was once again inclined at a 30-degree angle, ensuring close contact between the roots and the DOS gel. After deployment of 2, 12 and 24 h, the rhizotrons were carefully placed vertically in front of the PO imaging system to obtain triplicates of the DO fluorescence images (Supporting Information Note 2). After a deployment time of 24 h, the film was carefully retrieved for chemical imaging of labile P using a modified coloration-CID method in Supporting Information Note 3.

2.4. Image processing and DOS calibration

Acquired raw format images of O_2 were first split into red, green, and blue channels, and the corresponding ratio images were subsequently achieved by dividing the red channel (emission of the O_2-sensitive dye) with the green channel (emission of the reference dye) using the ImageJ 1.46 software (freely downloadable at https://imagej.net). Afterward, the ratio images were fitted with a previously obtained calibration curve, and then converted into O_2 concentrations (C, μM) as matrices. An area-specific three-point calibration procedure (Supporting Information Note 4) was conducted *in situ* before each O_2 imaging to confirm the accuracy of O_2 measurements in the rhizosphere (Rickelt et al., 2013).

To quantify the labile P images, the scanned images of labile P were first processed into gray-value images and corrected for any background effect. Afterward, the sequential gray-value matrices were fitted with gray-value versus a labile P concentration

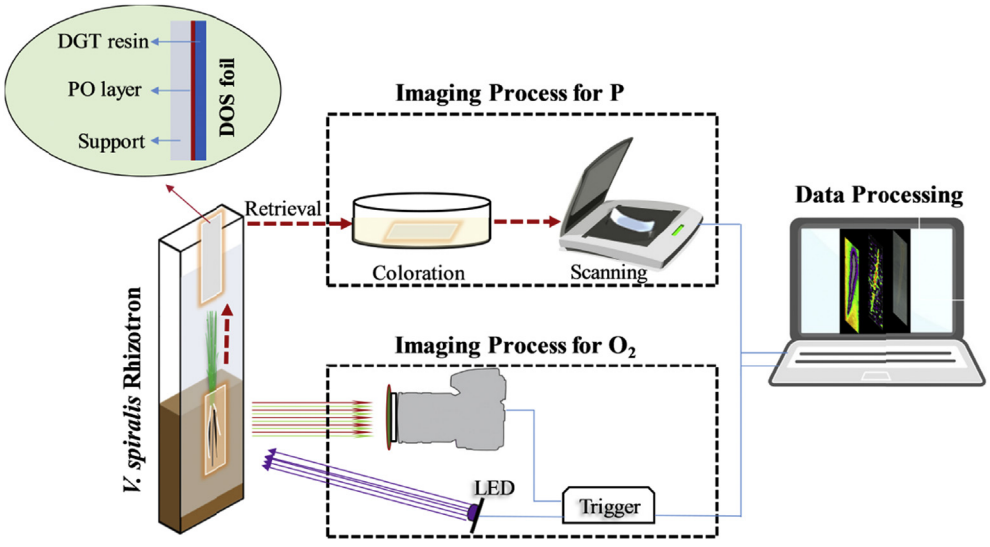

Fig. 1. Schematic overview for root-induced DO concentration and P flux imaging.

calibration curve and then converted into labile P flux (F, pg cm^{-2} s^{-1}) as matrices (see detailed description in the Supporting Information, Note 5-7; Fig. S2).

2.5. Date evaluation

The resulting O_2 concentrations and labile P fluxes as matrices were finally converted into 2-D images using the image processing software, SURFER 12.0, and MATLAB® 7.0. The major physico-chemical parameters including the total organic content (TOC), sediment porosity (φ), total P, dissolved reactive P in sediment (DRP_s) and in overlying water (DRP_w), O_2 penetration depth (OPH), diffusive O_2 uptake ($J_{(z)}$ and average volume-specific O_2 consumption (R_{SWI}) were quantified according to methods as described in Supporting Information Note 8. All point and 1-D data extracted from the images were represented as "mean ± standard deviation (SD)." Statistical analyses were performed using one-way analysis of variance (ANOVA); differences were not considered significant if $p > 0.05$.

3. Results and discussion

3.1. Chemical properties of the sediment and water

The basic characteristics of the sediment and water are summarized in Table S1. Obviously, the investigated sediment was characterized as silty sand with a high porosity (φ) of 0.65 (±0.09) and a low total organic matter (TOC) of 5.70% (±0.02), which was highly contaminated with P due to excessive input of anthropogenic nutrients (Han et al., 2013). The average OPH, $J_{(z)}$ and R_{SWI}, as calculated from the planar optode images, were 0.48 cm (±0.15), 22.49 nmol m^{-2} s^{-1} (±3.12) and 4.64 μmol m^{-3} s^{-1} (±1.07), which agreed with values measured in other freshwater sediments (Minett et al., 2013; Tian et al., 2015; Han et al., 2016).

To serve as a control, the 2-D spatial co-distributions of DO concentration and labile P flux imaged by DOS were measured prior to transplanting (Fig. 2). The semitransparent nature of DOS foil allows visual observation of distinct structures of geochemical interest, such as the sediment-water interface and root-sediment interface within the rhizotron (Fig. 2-A). O_2 and labile P were relatively uniformly distributed within the overlying water and sediment, but highly gradient distributions near the sediment-water interface (SWI) were observed. DO concentrations were generally measured to be about 180 μmol l^{-1} in the overlying water, followed by a stepwise decrease until it became unmeasurable below the depth of −0.6 cm. In contrast, the labile P flux distribution had a distinct pattern, reflected by a relatively stable and low level in the overlying water, followed by a consistent increase up to an average level of 128 pg cm^{-2} s^{-1} within the sediment (Fig. 2-D).

3.2. 2D co-distributions of O_2 and P in the rhizosphere of young single V. spiralis root

2D co-distributions of DO concentrations and labile P fluxes surrounding a 3-day-old *V. spiralis* root, which appeared to be root-like structures, are visualized in Fig. 3. Within 3 days, the root being studied grew 26.5 mm across the sensor foil, corresponding to an average growth rate of 0.37 mm h^{-1}. This growth rate is comparable to those reported by Liu et al. (2014) and Han et al. (2016), indicating that the chemistry of the DOS had no negative effects on the vitality of the roots. It is apparent that the distributions of DO and labile P are highly heterogeneous in the *V. spiralis* rhizosphere, which further highlights the benefit of measuring 2D distributions at the appropriate scale for those rhizosphere processes.

In the bulk sediment, the DO concentrations represented in the black regions in Fig. 3-B are nearly absent. A visible aerobic sphere with a width of approximately 2.0 mm, represented by the green-to-red colors, was developed surrounding the root. Hotspots of DO concentrations (up to 78 μM) were distributed brokenly on the root surface, which may be closely linked to the root-induced ROL along the entire root length (Frederiksen and Glud, 2006; Han et al., 2016). Labile P flux distribution exhibited a distinct pattern and was affected more significantly than the DO distribution. As shown in Fig. 3-C, labile P flux was generally unmeasurable in the region next to the individual root surface, reflecting localized P concentration minima, but thereafter increased gradually around the border of

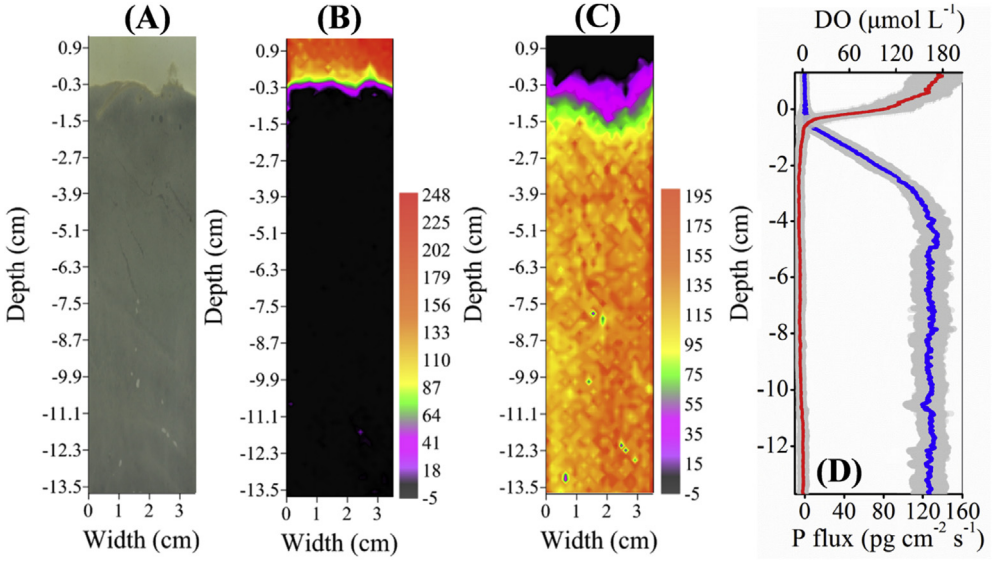

Fig. 2. Representative co-distributions of DO concentrations (μM) and labile P fluxes (pg cm^{-2} s^{-1}) near the sediment-water interface (SWI) in the rhizotron without the planted *V. spiralis*: (A) shows a photograph of the visible SWI through the transparent rhizotron window and the DOS; (B) gives corresponding 2-D images of DO concentrations, and (C) projects labile P fluxes; In D, the laterally-average depth profiles of DO and labile P fluxes are shown with the error bar indicated as a gray-shaded area, representing the standard deviations of the mean (N = 1490 for DO and N = 820 for labile P flux). The dotted line represents the approximate location of the SWI.

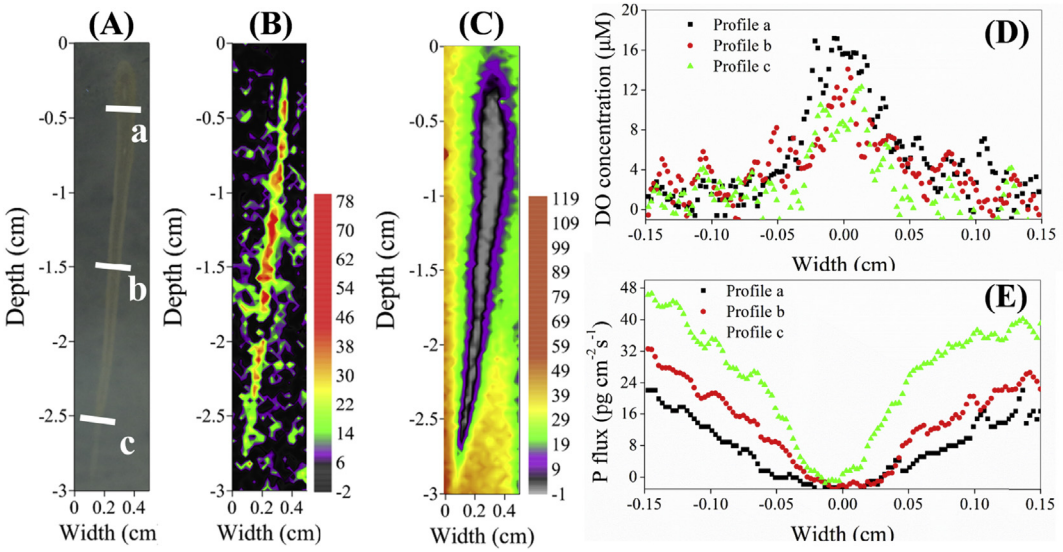

Fig. 3. (A) Represents a simple schematic of the individual *V. spiralis* root. (B) Represents the corresponding spatial co-distributions of DO concentrations (μM) and (C) represents the labile P fluxes (pg cm^{-2} s^{-1}) along the *V. spiralis* root three days after planting and 24 h after DOS application. (D) and (E) show the extracted O_2 and P profiles (a, b, c) from the corresponding B and C images, respectively, and (A) indicates the positions of the profiles.

the individual *V. spiralis* root to the background flux of ca.120 pg $cm^{-2}s^{-1}$ in the nearly anoxic condition of the bulk sediment. Similar patterns of P have also been imaged in the rhizosphere of plants such as *Brassica napus L.* and *Zea mays L.* (Kreuzeder et al., 2013; Santner et al., 2012).

Fig. 3-D and E show more detailed transect profiles of DO concentrations and labile P fluxes across different positions of the root surfaces (denoted by the white dots shown in Fig. 3-A). Two pronounced inverse gradients of DO concentration and labile P flux from the root towards the bulk sediment are first revealed simultaneously. Overall, the DO concentration maxima from profiles were always present on the root surface. Thereafter DO concentrations decreased exponentially from the root surface downward to the bulk sediment. By contrast, the profile of the labile P exhibited a distinct pattern corresponding to that of DO. The extent of P depletion was fairly constant within a distance of ca. 2 mm around the roots. The spatial changes of DO concentrations and labile P fluxes as a function of distance from the base of the root toward the root tip show clear differences ($p < 0.01$), which is reflected by a decreasing average O_2 concentration from 9.89 ± 5.02 μM to 3.68 ± 2.02 μM when approaching the root tip, with a corresponding increase of average labile P fluxes from 10.5 ± 5.79 pg cm^{-2} s^{-1} to 28.44 ± 11.60 pg cm^{-2} s^{-1}.

As evaluated from the data sets above and from another exemplary experiment with results at the same age are presented in Fig. S3. Here, the decreased P mobilization clearly corresponds to the O_2 enhancement in the rhizosphere of young *V. spiralis*. This observation seems to confirm the expected coupling relationship that P mobilization is largely regulated by root-mediated ROL. The diminished fluxes of labile P in the rhizosphere indicates a depletion of DGT-labile P resulting from various root activities such as P uptake or sorptive P fixation (Hupfer and Dollan, 2003; Santner et al., 2012). It has been reported that the amount of P directly taken in by roots accounted for less than 5 percent of the P depletion in the rhizosphere, and it would be expected that most of the porewater P depletion would be immobilized rather than assimilated in the rhizosphere vicinity (Ahmed et al., 2016; Lambers et al., 2006). During the quick elongation of new roots within the anaerobic sediment, the conspicuously produced O_2 was translocated to the roots and then diffused into the immediate surrounding sediment, resulting in the gradual formation of metallic oxides (e.g., iron and manganese oxyhydroxides) around the roots (Jovanovic et al., 2015; Koop-Jakobsen and Wenzhofer, 2015). Such freshly formed oxides acted as highly reactive surfaces for rapidly trapping labile P by adsorption, and consequently somewhat reducing the localized P mobilization near a single root (Pages et al., 2011).

3.3. 2D co-distributions of O_2 and P in the rhizosphere over a diurnal change

Fig. 4 presents 2D representative co-distributions of DO concentrations and labile P fluxes at the sub-mm scale during day and night deployment. At the night-time deployment, the O_2 images revealed a large area of O_2 absence that was mapped over the entire rhizosphere of the 21-day-old *V. spiralis*, and only a small and patchy area of elevated DO concentrations ranging from 16 μM to 34 μM was restricted to the partial *V. spiralis* roots surface (Fig. 4-A). Correspondingly, DGT-measured labile P was strongly depleted in the immediate main root vicinity and showed a clearly increasing gradient penetrating the surrounding bulk sediment (Fig. 4-B), which resembled rhizosphere P distributions on Day 3. However, during the whole day of deployment, much higher O_2 leakage occurred locally around the roots with peak DO concentrations of 100 μM or greater (Fig. 4-C). The distribution of the labile P fluxes during the daytime was much like that at night, except for the increased P-depletion zones occurring around the base roots and among the root tips (Fig. 4-D). The overall aerobic microniches measured at the probe interface reached a larger size of ca.7.9 cm^2 during the daytime, compared to nighttime (approximately 3.8 cm^2). Meanwhile, a visual zone of P depletion near the *V. spiralis* roots was unexpectedly larger, extending about 6–15 mm into the bulk sediment and accounting for approximately 60% of the probe surface (17.1 cm^2). It was also noted that the major influence of root-induced P depletion during the daytime as compared to nighttime was restricted to the regions of the root zone aerobic and anaerobic interface (along the border of rhizosphere), while the major root zone remained unchanged.

To gain a better insight into changes of the studied species, the depth-averaged profiles of DO concentrations and labile P fluxes

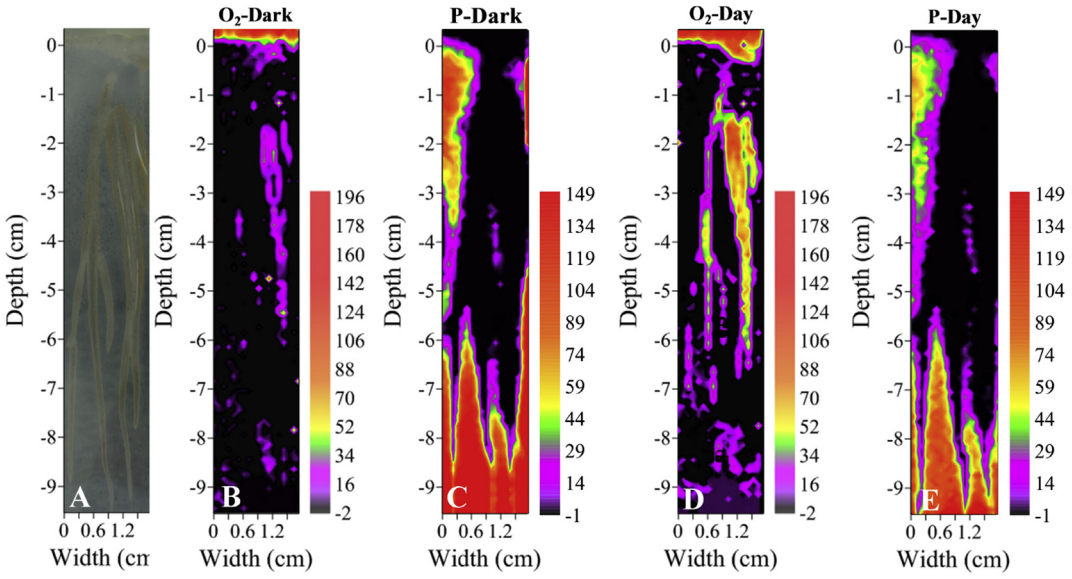

Fig. 4. An example of a 21-day-old *V. spiralis* root (A) and the corresponding spatial co-distributions of DO concentrations (μM) and labile P fluxes (pg cm^{-2} s^{-1}) during night-time (0 μmol photos m^{-2} s^{-1}, B and C) and daytime (216 μmol photos m^{-2} s^{-1}, D and E) deployments.

during the night and day time cycles were extracted from their corresponding images (Fig. 4) and are shown in Fig. 5.

Fig. 5 reveals a sharp decrease of DO concentrations from about ~150 μm over the SWI down to zero over distances routinely covered within the uppermost 10 mm. The sediment remained anoxic as the depth increased. We also observed another oxygen zonation between the depths of 13.2 mm and 33.6 mm across the day profile, which coincides with 2D observations of root-associated DO changes (Fig. 5-A, C). The average depth profiles of P showed that the labile P fluxes during the night and day time generally remained at a low level with the aerobic overlying water and ROL-induced oxygenated sediments at depths from 0 to 60 mm, except for a slight increase in P fluxes in the top 5 mm of sediment depth. Thereafter, the averaged fluxes during the night and day increased rapidly up to almost 160 pg cm^{-2} s^{-1} and 100 pg cm^{-2} s^{-1} at ~98.6 mm depth, respectively (Fig. 5-B, D).

As evaluated from above data sets, a pronounced diurnal rhythm for O_2 availability along and outward from *V. spiralis* roots was first revealed. Diurnal rhythms of O_2 leakage and rhizosphere oxygenation follow patterns much like other terrestrial/aquatic plants, i.e., *Vigna unguiculata* (Rao et al., 2002); *Thalassia testudinum* (Borum et al., 2005); *Juncus effuses L.* (Blossfeld and Gansert, 2007) and *Lobelia* (Lenzewski et al., 2018). The intense ROL during the daytime should be attributed to the photosynthesis-derived O_2 production, while the weak ROL around the basal roots at night was due to the O_2 diffusion from the aerated water via plant aerenchyma (Han et al., 2016; Koren et al., 2015; Wang et al., 2014). This continuous rhizosphere oxygenation over the course of a day is an important mechanism by which terrestrial/aquatic plants can reduce exposure to phytotoxins, like reduced sulphide and ferrous species (Laskov et al., 2006). Therefore, its physiological benefit could be possibly responsible for *V. spiralis* emergence as a formidable invasive species in areas where they have been introduced. In contrast to DO, *V. spiralis* exhibited no visible diurnal rhythm in rhizosphere labile P flux. The resulting P images revealed only slight differences in response to the day-to-night-transition with no differences in the P-depletion zone nor in the minimum flux for most of the *V. spiralis* rhizosphere. The impact was generally restricted to a small area in the immediate vicinity of the rhizosphere and non-rhizosphere boundary (Fig. 4-C, 4E). This is most likely due to the enhanced ROL rates during the daytime favoring the gradual amplification of the oxic and anoxic interface along

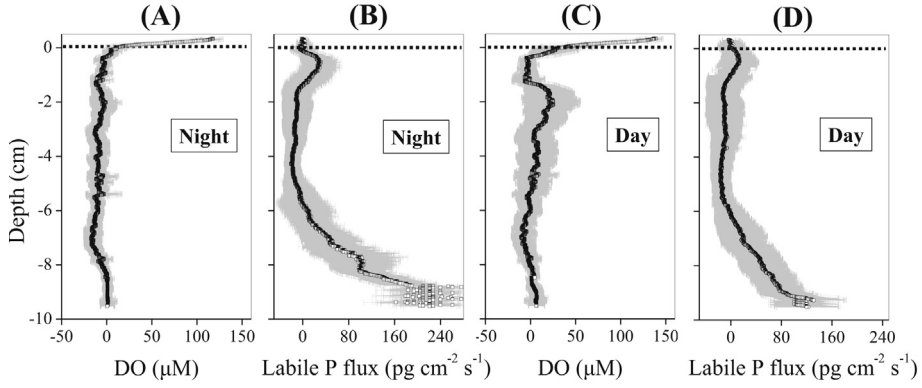

Fig. 5. 1-D profiles of the depth-averaged DO concentration (μM) and labile P flux (pg cm^{-2} s^{-1}) during night-time (A and B) and daytime (C and D) deployments. The black dotted lines represent approximate location of the SWI. The laterally-averaged depth profiles of DO and labile P fluxes (D), with the error bar shown as the gray-shaded area, represent the standard deviations of the mean (N = 748 for DO and N = 399 for labile P flux).

with the greater P depletion from precipitation of iron (III) oxyhydroxides and the uptake by the root and aerobic bacteria. Similar diurnal fluctuations have also been observed in P porewater in the rhizosphere of *Zostera capricorni* or eel grass (Pages et al., 2012). Moreover, the remarkably wide depletion zone of P observed in the surroundings of *V. spiralis* roots (>4 mm, Fig. 4) over a diurnal cycle, indicates that P mobilization was significantly restrained, which further supports the widely-accepted concept that submerged plants can effectively prevent P release to the overlying water (Horppila and Nurminen, 2003; Hupfer and Dollan, 2003).

3.4. Dynamics of interactions between O_2 and P in the rhizosphere of *V. spiralis*

The observed coincidence of P-depletion and ROL zones around the younger *V. spiralis* roots, suggested that rhizosphere P availability might be primarily controlled by ROL (Fig. 3 and Fig. S3). In contrast, zones of P depletion induced by the older root *V. spiralis* apparently outlined the O_2-availability zones (Fig. 4). Similar patterns were also replicated as observed in Fig. S4. As mentioned earlier, the visible P-depletion zone around the roots can reflect the pronounced changes of oxygenated zone, meanwhile the changes of oxygenated zone were primarily depend on the balance between ROL rates and diverse O_2-consumption processes (e.g. microbial respiration, chemical oxidation and organic degradation) (Frederiksen and Glud, 2006; Jensen et al., 2005). Our previous studies confirmed that young *V. spiralis* from Days 3–9 exhibited much higher ROL rates than those recorded in Days 18–36 (Han et al., 2016). Lemoine et al. (2012) also measured enhanced ROL rates of *V. spiralis* rooting in the freshly anaerobic sediment as compared to more oxygenated sediments. Accordingly, O_2 leakage into the immediate rhizosphere by the younger *V. spiralis* root appeared to be enough to maintain oxic microniches and sustain P-depletion processes. It can also explain why the detectable O_2-availability zone around the older *V. spiralis* roots in the pseudo-color images is actually several millimeters narrower than the ROL-induced oxygenated zone.

To gain a better insight into interactions between P and O_2, the patterns of ROL-induced changes in the oxygenation zone and labile P flux around the *V. spiralis* root are described in Fig. 6. As illustrated, the radial O_2 distributions around a single root are most often assumed to be elliptical (Frederiksen and Glud, 2006; Minett et al., 2013). We hypothesize that the continuous O_2 leakage and diffusion into the surrounding sediments in the *V. spiralis* can lead

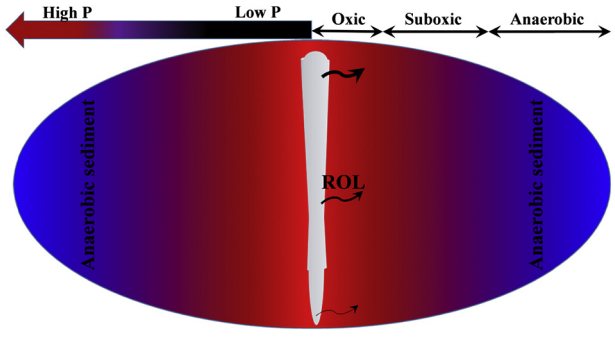

Fig. 6. The idealized patterns of ROL-induced changes in the oxygenation zone and labile P flux in the *V. spiralis* rhizosphere. The oxic zone is root-adjacent (the red area), the suboxic zone is the layer where the redox gradient is evident (where the red starts blending into purple area), and the anaerobic zone is shown as the layer unaffected by the root activities (indicated as the blue area). The width scale is arbitrary. (For interpretation of the references to color in this figure legend, the reader is referred to the Web version of this article.)

to three different "ROL-barrier" redox layers within the entire rhizosphere: 1) the oxic layer with only a slight or no radial O_2 diffusive resistance, 2) the suboxic layer with a greater but attenuated radial O_2 diffusive resistance, and 3) the anaerobic layer with the greatest and most notably steady radial O_2 diffusive resistance. As O_2 diffuses continuously from the root surface, through the oxic zone of submerged sediment to an adjacent oxidization zone, metallic oxyhydroxides gradually form, which consequently reduces the localized P mobilization in the surrounding sediment around the roots. When the continuous O_2 leakage penetrates the already oxidized sediment, the O_2 is less subject to the barrier effects, which gradually expands the oxygenated zone as the roots progressively age (Han et al., 2016). This was further supported by the present findings of the formation of visible brown metallic oxides layers adjacent to the *V. spiralis* roots (Figs. 3-A and 4-A, Fig.s S3-A and S4-A). These metallic oxides are composed mainly of iron (III) oxyhydroxides and are always referred to as Fe plaque. They have a high specific surface and a high affinity for adsorbing phosphates, and they act as an effective reservoir for rhizosphere sediment P (Hansel et al., 2001; Mi et al., 2013). In the stabilized oxic and partial suboxic zones, the sediment P may be largely "locked up" and slightly affected by irradiance and root age due to its high affinity with metallic oxides. This may largely explain the broader P-depletion zone seen in a substantial part of the rhizosphere of 21-day old *V. spiralis*. As the root growth progressed, enhanced aerobe activities were likely attenuating P mobilization within the older *V. spiralis* rhizosphere (Wigand and Stevenson, 1997). However, this effect is too small to explain the strong P depletion within the rhizosphere.

In addition to regulating rhizospheric P immobilization, other viewpoint showed that the physiological benefit of ROL-derived sediment oxygenation was also a mechanism that could promote P mobilization into the rhizospheric solution and sustain the plant's nutrient requirements. Brodersen et al., 2016; Brodersen et al., 2017 have demonstrated that ROL-induced sediment oxygenation in the immediate rhizosphere of the macrophytes, *Zostera marina* and *Cymodocea serrulata* can cause rhizosphere acidification due to the continued proton (H^+) production from the sulfide oxidation and the precipitation of iron (III) oxyhydroxides, thereby resulting in the release and uptake of previously sequestered P. Meanwhile the ROL-induced stimulation of microbial activities as well as the release of root exudates could have contributed to the P liberation from the iron (III) oxyhydroxide captured P in the oxygenated rhizosphere sediments (Mei et al., 2014). Still, a net P immobilization of P in the rhizosphere was developed, which we hypothesize is due to the rapid P immobilization by adsorption working faster than its concomitant bioavailable P release.

4. Conclusions

In this work, we used a disturbance-free DOS imaging method for simultaneous visualization of the dynamics of O_2 and P availabilities in the *V. spiralis* rhizosphere, which provided a fascinating view of ROL-driven sediment oxygenation and the associated root-mediated P migration in the rhizosphere. Their spatiotemporal co-distribution patterns showed significant small-scale heterogeneity, further highlighting the complexity of such a dynamic ecosystem and the advantage of the high-resolution imaging methods. 2D co-distributions for the young *V. spiralis* roots revealed a more significant coupling relationship between O_2 and P as compared to those for the older root. In addition, we first revealed their co-distribution patterns around *V. spiralis* root over a diurnal cycle, which was reflected by a pronounced diurnal rhythm for O_2 availability, but with no significant diurnal rhythm for P availability. To elucidate such phenomena, we proposed three different "ROL-barrier" redox

layers formed within the entire rhizosphere being responsible for P-availability regulation. Overall, our results adequately revealed that the *V. spiralis* rhizosphere was a P sink maintained by the ROL process. This study advances our understanding in the field of predictive O_2 and P modeling, which includes root co-distribution patterns over a diurnal cycle and provides additional information on the rhizosphere process, as well as the phytoremediation mechanisms of P-limited eutrophic lakes by submerged macrophytes.

Acknowledgements and Funding Sources

This work was supported by the National Science Foundation of China (No. 41773087) the Jiangsu Natural Science Foundation (No. BK20171075), and the Key Laboratory of Soil Environment and Pollution Remediation, Institute of Soil Science, Chinese Academy of Sciences (SEPR2017-11).

Appendix A. Supplementary data

Supplementary data related to this article can be found at https://doi.org/10.1016/j.chemosphere.2018.05.180.

References

Ahmed, S., Klassen, T.N., Keyes, S., Daly, M., Jones, D.L., Mavrogordato, M., Sinclair, I., Roose, T., 2016. Imaging the interaction of roots and phosphate fertiliser granules using 4D X-ray tomography. Plant Soil 401, 125–134.

Armstrong, W., Cousins, D., Armstrong, J., Turner, D.W., Beckett, P.M., 2000. Oxygen distribution in wetland plant roots and permeability barriers to gas-exchange with the rhizosphere: a microelectrode and modelling study with *Phragmites australis*. Ann. Bot 86, 687–703.

Blossfeld, S., Gansert, D., 2007. A novel non-invasive optical method for quantitative visualization of pH dynamics in the rhizosphere of plants. Plant Cell Environ. 30, 176–186.

Borum, J., Pedersen, O., Greve, T.M., Frankovich, T.A., Zieman, J.C., Fourqurean, J.W., Madden, C.J., 2005. The potential role of plant oxygen and sulphide dynamics in die-off events of the tropical seagrass, *Thalassia testudinum*. J. Ecol. 93, 148–158.

Brodersen, K.E., Koren, K., Lichtenberg, M., Kuhl, M., 2016. Nanoparticle-based measurements of pH and O2 dynamics in the rhizosphere of *Zostera marina L.*: effects of temperature elevation and light-dark transitions. Plant Cell Environment 39, 1619–1630.

Brodersen, K.E., Koren, K., Mosshammer, M., Ralph, P.J., Kuhl, M., Santner, J., 2017. Seagrass-mediated phosphorus and iron solubilization in tropical sediments. Environ. Sci. Technol. 51, 14155–14163.

Cao, X., Wang, Y.Q., He, J., Luo, X.Z., Zheng, Z., 2016. Phosphorus mobility among sediments, water and cyanobacteria enhanced by cyanobacteria blooms in eutrophic Lake Dianchi. Environ. Pol. 219, 580–587.

Cheng, X.Y., Wang, M., Zhang, C.F., Wang, S.Q., Chen, Z.H., 2014. Relationships between plant photosynthesis, radial oxygen loss and nutrient removal in constructed wetland microcosms. Biochem. Systemat. Ecol. 54, 299–306.

Frederiksen, M.S., Glud, R.N., 2006. Oxygen dynamics in the rhizosphere of *Zostera marina*: a two-dimensional planar optode study. Limnol. Oceanogr. 51, 1072–1083.

Guan, D.-X., Williams, P.N., Xu, H.-C., Li, G., Luo, J., Ma, L.Q., 2016. High-resolution measurement and mapping of tungstate in waters, soils and sediments using the low-disturbance DGT sampling technique. J. Hazard Mater. 316, 69–76.

Han, C., Ding, S.M., Yao, L., Shen, Q.S., Zhu, C.G., Wang, Y., Xu, D., 2015. Dynamics of phosphorus–iron–sulfur at the sediment–water interface influenced by algae blooms decomposition. J. Hazard Mater. 300, 329–337.

Han, C., Geng, J.J., Ren, H.Q., Gao, S.X., Xie, X.C., Wang, X.R., 2013. Phosphite in sedimentary interstitial water of Lake Taihu, a large eutrophic shallow lake in China. Environ. Sci. Technol. 47, 5679–5685.

Han, C., Ren, J.H., Tang, H., Xua, D., Xie, X.C., 2016. Quantitative imaging of radial oxygen loss from *Valisneria spiralis* roots with a fluorescent planar optode. Sci. Total Environ. 569, 1232–1240.

Han, C., Ren, J.H., Wang, Z.D., Tang, H., Xu, D., 2017. A novel hybrid sensor for combined imaging of dissolved oxygen and labile phosphorus flux in sediment and water. Water Res. 108, 179–188.

Hansel, C.M., Fendorf, S., Sutton, S., Newville, M., 2001. Characterization of Fe plaque and associated metals on the roots of mine-waste impacted aquatic plants. Environ. Sci. Technol. 35, 3863–3868.

Hoefer, C., Santner, J., Borisov, S.M., Wenzel, W.W., Puschenreiter, M., 2017. Integrating chemical imaging of cationic trace metal solutes and pH into a single hydrogel layer. Anal. Chim. Acta 950, 88–97.

Horppila, J., Nurminen, L., 2003. Effects of submerged macrophytes on sediment resuspension and internal phosphorus loading in Lake Hiidenvesi (southern Finland). Water Res. 37, 4468–4474.

Huang, W., Chen, Q.W., Ren, K.X., Chen, K.N., 2015. Vertical distribution and retention mechanism of nitrogen and phosphorus in soils with different macrophytes of a natural river mouth wetland. Environ. Monit. Assess. 187.

Hupfer, M., Dollan, A., 2003. Immobilisation of phosphorus by iron-coated roots of submerged macrophytes. Hydrobiologia 506, 635–640.

Jensen, S.I., Kuhl, M., Glud, R.N., Jorgensen, L.B., Prieme, A., 2005. Oxic microzones and radial oxygen loss from roots of *Zostera marina*. Mar. Ecol. Prog. Ser. 293, 49–58.

Jovanovic, Z., Pedersen, M.O., Larsen, M., Kristensen, E., Glud, R.N., 2015. Rhizosphere O_2 dynamics in young *Zostera marina* and *Ruppia maritima*. Mar. Ecol. Prog. Ser. 518, 95–105.

Ke, X.S., Li, W., 2006. Germination requirement of *Vallisneria natans* seeds: implications for restoration in Chinese lakes. Hydrobiologia 559, 357–362.

Koop-Jakobsen, K., Wenzhofer, F., 2015. The dynamics of plant-mediated sediment oxygenation in *Spartina anglica* rhizospheres-a planar optode study. Estuar. Coast 38, 951–963.

Koop-Jakobsen, K., Fischer, J., Wenzhofer, F., 2017. Survey of sediment oxygenation in rhizospheres of the saltmarsh grass - *Spartina anglica*. Sci. Total Environ. 589, 191–199.

Koren, K., Brodersen, K.E., Jakobsen, S.L., Kuhl, M., 2015. Optical sensor nanoparticles in artificial sediments-a new tool to vsualize O_2 dynamics around the rhizome and roots of seagrasses. Environ. Sci. Technol. 49, 2286–2292.

Kreuzeder, A., Santner, J., Prohaska, T., Wenzel, W.W., 2013. Gel for simultaneous chemical imaging of anionic and cationic solutes using diffusive gradients in thin films. Anal. Chem. 85, 12028–12036.

Kuzyakov, Y., Blagodatskaya, E., 2015. Microbial hotspots and hot moments in soil: concept & review. Soil Biol. Biochem. 83, 184–199.

Lai, W.L., Zhang, Y., Chen, Z.H., 2012. Radial oxygen loss, photosynthesis, and nutrient removal of 35 wetland plants. Ecol. Eng. 39, 24–30.

Lambers, H., Shane, M.W., Cramer, M.D., Pearse, S.J., Veneklaas, E.J., 2006. Root structure and functioning for efficient acquisition of phosphorus: matching morphological and physiological traits. Ann. Bot 98, 693–713.

Larsen, M., Santner, J., Oburger, E., Wenzel, W.W., Glud, R.N., 2015. O_2 dynamics in the rhizosphere of young rice plants (*Oryza sativa L.*) as studied by planar optodes. Plant Soil 390, 279–292.

Laskov, C., Horn, O., Hupfer, M., 2006. Environmental factors regulating the radial oxygen loss from roots of *Myriophyllum spicatum* and *Potamogeton crispus*. Aquat. Bot. 84, 333–340.

Lemoine, D.G., Mermillod-Blondin, F., Barrat-Segretain, M.H., Masse, C., Malet, E., 2012. The ability of aquatic macrophytes to increase root porosity and radial oxygen loss determines their resistance to sediment anoxia. Aquat. Ecol. 46, 191–200.

Lenzewski, N., Mueller, P., Meier, R.J., Liebsch, G., Jensen, K., Koop-Jakobsen, K., 2018. Dynamics of oxygen and carbon dioxide in rhizospheres of *Lobelia dortmanna* - a planar optode study of belowground gas exchange between plants and sediment. New Phytol. https://doi.org/10.1111/nph.14973.

Liang, S., Guan, D.X., Ren, J.H., Zhang, M., Luo, J., Ma, L.Q., 2014. Effect of aging on arsenic and lead fractionation and availability in soils: coupling sequential extractions with diffusive gradients in thin-films technique. J. Hazard Mater. 273, 272–279.

Liu, H.Y., Meng, F.B., Tong, Y.D., Chi, J., 2014. Effect of plant density on phytoremediation of polycyclic aromatic hydrocarbons contaminated sediments with *Vallisneria spiralis*. Ecol. Eng. 73, 380–385.

Luo, J., Cheng, H., Ren, J., Davison, W., Zhang, H., 2014. Mechanistic insights from DGT and soil solution measurements on the uptake of Ni and Cd by *Radish*. Environ. Sci. Technol. 48, 7305–7313.

Luo, J., Yin, D.X., Cheng, H., Davison, W., Zhang, H., 2018. Plant induced changes to rhizosphere characteristics affecting supply of Cd to *Noccaea caerulescens* and Ni to *Thlaspi goesingense*. Environ. Sci. Technol. 52, 5085–5093.

Luo, J., Zhang, H., Santner, J., Davison, W., 2010. Performance characteristics of diffusive gradients in thin films equipped with a binding gel layer containing precipitated ferrihydrite for measuring arsenic(V), selenium(VI), vanadium(V), and antimony(V). Anal. Chem. 82, 8903–8909.

Mei, X.Q., Yang, Y., Tam, N.F.Y., Wang, Y.W., Li, L., 2014. Roles of root porosity, radial oxygen loss, Fe plaque formation on nutrient removal and tolerance of wetland plants to domestic wastewater. Water Res. 50, 147–159.

Mi, W., Cai, J., Tuo, Y., Zhu, H., Hua, Y., Zhao, J., Zhou, W., Zhu, D., 2013. Distinguishable root plaque on root surface of *Potamogeton crispus* grown in two sediments with different nutrient status. Limnology 14, 1–11.

Minett, D.A., Cook, P.L.M., Kessler, A.J., Cavagnaro, T.R., 2013. Root effects on the spatial and temporal dynamics of oxygen in sand-based laboratory-scale constructed biofilters. Ecol. Eng. 58, 414–422.

Pages, A., Teasdale, P.R., Robertson, D., Bennett, W.W., Schafer, J., Welsh, D.T., 2011. Representative measurement of two-dimensional reactive phosphate distributions and co-distributed iron(II) and sulfide in seagrass sediment porewaters. Chemosphere 85, 1256–1261.

Pages, A., Welsh, D.T., Robertson, D., Panther, J.G., Schafer, J., Tomlinson, R.B., Teasdale, P.R., 2012. Diurnal shifts in co-distributions of sulfide and iron(II) and profiles of phosphate and ammonium in the rhizosphere of *Zostera capricorni*. Estuar. Coast Shelf Sci. 115, 282–290.

Pan, Y., Guan, D.X., Zhao, D., Luo, J., Zhang, H., Davison, W., Ma, L.Q., 2015. Novel speciation method based on diffusive gradients in thin-films for *in situ* measurement of Cr-VI in aquatic systems. Environ. Sci. Technol. 49, 14267–14273.

Rao, T.P., Yano, K., Iijima, M., Yamauchi, A., Tatsumi, J., 2002. Regulation of

rhizosphere acidification by photosynthetic activity in cowpea (*Vigna unguiculata L. Walp.*) seedlings. Ann. Bot 89, 213–220.
Razavi, B.S., Zarebanadkouki, M., Blagodatskaya, E., Kuzyakov, Y., 2016. Rhizosphere shape of *lentil* and *maize*: spatial distribution of enzyme activities. Soil Biol. Biochem. 96, 229–237.
Rickelt, L.F., Askaer, L., Walpersdorf, E., Elberling, B., Glud, R.N., Kuhi, M., 2013. An optode sensor array for long-term *in situ* oxygen measurements in soil and sediment. J. Environ. Qual. 42, 1267–1273.
Santner, J., Larsen, M., Kreuzeder, A., Glud, R.N., 2015. Two decades of chemical imaging of solutes in sediments and soils - a review. Anal. Chim. Acta 878, 9–42.
Santner, J., Zhang, H., Leitner, D., Schnepf, A., Prohaska, T., Puschenreiter, M., Wenzel, W.W., 2012. High-resolution chemical imaging of labile phosphorus in the rhizosphere of *Brassica napus L.* cultivars. Environ. Exp. Bot. 77, 219–226.
Schelske, C.L., 2009. Eutrophication: focus on phosphorus. Science 324, 722–722.
Soana, E., Bartoli, M., 2013. Seasonal variation of radial oxygen loss in *Vallisneria spiralis L.*: an adaptive response to sediment redox? Aquat. Bot. 104, 228–232.
Sondergaard, M., Bjerring, R., Jeppesen, E., 2013. Persistent internal phosphorus loading during summer in shallow eutrophic lakes. Hydrobiologia 710, 95–107.
Sondergaard, M., Jensen, J.P., Jeppesen, E., 2003. Role of sediment and internal loading of phosphorus in shallow lakes. Hydrobiologia 506, 135–145.
Tian, C.C., Wang, C.B., Tian, Y.Y., Wu, X.Q., Xiao, B.D., 2015. Root radial oxygen loss and the effects on rhizosphere microarea of two submerged plants. Pol. J. Environ. Stud. 24, 1795–1802.
Wang, W.L., Han, R.M., Wan, Y.J., Liu, B., Tang, X.Y., Liang, B., Wang, G.X., 2014. Spatio-temporal patterns in rhizosphere oxygen profiles in the emergent plant species *Acorus calamus*. PLoS One 9.
Williams, P.N., Santner, J., Larsen, M., Lehto, N.J., Oburger, E., Wenzel, W., Glud, R.N., Davison, W., Zhang, H., 2014. Localized flux maxima of arsenic, lead, and iron around root apices in flooded lowland rice. Environ. Sci. Technol. 48, 8498–8506.
Wigand, C., Stevenson, J.C., 1997. Facilitation of phosphate assimilation by aquatic mycorrhizae of *Vallisneria americana* Michx. Hydrobiologia 342–343, 35–41.
Zhou, C.Y., Guan, D.X., Williams, P.N., Luo, J., Ma, L.Q., 2016. Novel DGT method with tri-metal oxide adsorbent for *in situ* spatiotemporal flux measurement of fluoride in waters and sediments. Water Res. 99, 200–208.